ANNUAL REPORT

In Support of the Air Force Office Of Scientific Research Award No. FA9550-20-1-0025

Touchless Sensing of Electrostatic Potential and Material Characterization Using Neighboring Spacecraft

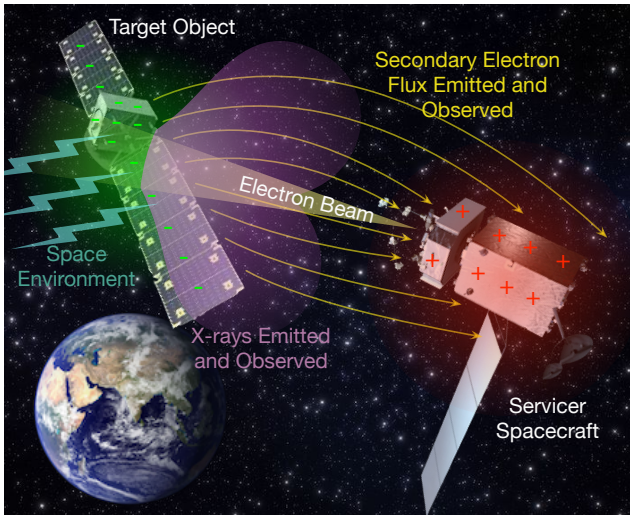

Dr. Hanspeter Schaub (PI)
Professor, Glenn L. Murphy Chair in Engineering
University of Colorado
Aerospace Engineering Sciences Department
Boulder, CO 80309-0429

January 21, 2021

Table of Contents

1 Project Overview

This 3-year research study completed its first year. The goal is to research touchless methods to sense neighboring spacecraft charge using either electron or x-ray measurements, as well as study the impact of charging on rendezvous and docking operations. The general concept is as follows. An inspector spacecraft is assumed to be station-keeping dozens of meters from a target space object and seeks to determine the relative charge of the target. This scenario is of interest to orbital inspection and servicing missions where differential charging is of concern during docking (electrostatic discharge) as well as to predict how the charged orbital perturbations impact relative motion guidance and control. The motivation for this work includes mission scenarios such as close proximity operations and vehicle inspection, servicing mission and GEO debris removal. The orbital servicing in particular is a hot topic right now with Northrop Grumman demonstrating the first autonomous docking and life-extension mission recently with the MEV-1 mission. Further, a particularly promising geosynchronous space debris mitigation method is the electrostatic tractor concept to touchlessly control relative motion or detumble an uncontrolled space object. Here touchless charge sensing has been identified as a key component of a charged relative orbit control solution to avoid bifurcations in the closed loop response. Being able to simultaneously sense the surface material property enables developing a surface charging model or making docking decisions depending on the surface composition. The target spacecraft is assumed to be flying outside the van Allen belts, such as at the geosynchronous orbit regime, where the Debye shielding effect of the ambient plasma is minimal.

The touchless charge and material property sensing methods involve both active irradiation of a conducting surface with electrons and measuring the resultant bremsstrahlung x-ray spectra or secondary electron emissions, as well as a passive sensing method using the natural space environment to stimulate these emissions. Both of these physical phenomena depend on the potential of the surface, thus the target potential can be inferred. In addition, x-ray and secondary electron characteristics are material dependent, allowing identification of material composition from the x-ray and plasma measurements. These two methods can be used in tandem, by utilizing an x-ray spectrometer and a plasma analyzer. The 3-year project will perform both numerical and extensive experimental research to study and analyze the charging accuracy on complex shapes with multiple surface properties. Each method has its strengths that can be fused into a joint filter to create a robust sensing solution.

The first project year successfully ramped up students onto the research tasks, upgraded the chamber to perform the large number of experiments to be performed, and made strong progress with a range of simulation and analysis tasks. The fall semester saw several exciting electron sensing experiments conducted where we are able to validate numerical analysis results studying the complex electron flux around non-spherical shapes. The vacuum chamber test facility has been upgraded with enhanced sensor sweeping capabilities, as well as new LabView-based chamber control software. The later allows for more automated data taking in long-running experiments.

A conference paper on the charged guidance and control of a servicer approaching to docking has received strong industry interest and feedback. It illustrates how a target object can begin to tumble because of electrostatic forces and torques exerted by the approaching servicer under a range of space weather conditions. Further, new research directions are being explored where a new beam expansion and deflection model has been developed, as well as pulsed charging/beaming techniques are being explored. The beam expansion and deflection work was done in collaboration with a Spanish professor, Dr. Gabriel Cano Gómez. It will be a critical tool in evaluating how well we can probe a neighboring spacecraft structure to determine its potential. The pulsed beaming research is looking at methods to excite a measurable electron or x-ray response without impacting the natural steady-state potential of the target surface. A paper was completed looking at the GEO environmental impacts on the x-ray charging concept and found that the environment itself could allow for charge sensing up to 1000 meters away, depending on the accuracy of the sensor. However, the x-rays generated in the spectrometer by the environmental electrons hitting the sensor itself can be a more limiting factor.

This annual report is composed as follows. Sections are included providing updates on the project travel, staffing and budget. Next a more detailed section includes a range of updates on the technical tasks. This is followed by a section listing all the associated publications. This is followed by a final section providing conclusions and outlook for the next project year.

2 Related Year 3 Travel

Many conferences trip were planned for the summer and fall of 2020, but these all got postponed, canceled or moved to a virtual online format. The program review meeting was also held in a virtual format. Thus, travel was light this year and included:

- March 2020, Kieran Wilson presented a paper at the IEEE aerospace conference in Big Sky, Montana

3 Staffing Update

The research grant contains support for two graduate research assistants (GRAs). Currently the primary GRAs are Kieran Wilson and Julian Hammerl. Further, other Ph.D. students Miles Bengtson and Álvaro Romero-Calvo supported this project in 2020. Miles is fully covered with an NDSEG fellowship while Álvaro is 80% covered by the La Caixa fellowship. This setup has allowed for a good overlap with the senior students Kieran and Miles and the newer students Julian and Álvaro who will take over full leadership of this work after summer 2021. The challenge is always how to ramp up students into a new project, as well as handle graduating senior students who are involved in this research. I'm pleased with how this project is going in that regard. The project student support funds have been applied in a manner to yield more graduate student support than originally envisioned. The transitions between graduating students and incoming students are going smoothly despite the COVID challenges.

Next is an outline of the details of the project staffing. Julian didn't start until the fall of 2021. Thus we were able to hire in a MS student Charlie Lipscomb to support the project in the spring as an hourly researcher. Álvaro participated part-time as a GRA in the spring and summer 2020 to have a good overlap with the outgoing Ph.D. student Miles Bengtson. Miles graduated in November 2020. In the fall of 2020 the undergraduate researcher Ryan Block joined this program as well. He is going to participate through the spring of 2021. Both Álvaro and Kieran are advising Ryan jointly. Julian started as a GRA in the fall of 2020 working on this project. However, due to COVID-related issues with the embassies being closed in Austria, like many other international students he was not able to get his Visa's in time to be on campus in time for the start of the Fall semester. Rather, he worked remotely on this project in the fall helping with simulation, pulsed charging analysis and experimental data processing. This gave him a good introduction to this project to enable rapid on-ramping on the experiments now that he arrived in Boulder, Colorado at the beginning of January. Kieran will remain the project GRA lead until he graduates at the end of the spring 2021 semester. After this Álvaro is setup to become the project GRA lead for the next academic year.

The list of the students involved in this research is:

- Kieran Wilson, a Ph.D. student who started in the fall of 2017. His is expected to graduate in the summer of 2021. He is interested in the charged astrodynamics research and his dissertation is on the x-ray sensing technique of touchless charge sensing, as well as the GNC implication for rendezvous and docking.
- Julian Hammerl, a Ph.D. student who started in the fall of 2020. He has started working on this AFOSR project in August 2020. His dissertation research is on the charged relative motion control for close proximity operations and debris mitigation. After Kieran graduates this summer Julian will be take over the x-ray charge sensing method research as well as the charged relative motion GNC work.
- Álvaro Romero Calvo, a Ph.D. student who started in the fall of 2019. His dissertation research is on the use of electrostatic and magnetic fields in space applications. He is partially supported on the La Caixa fellowship and partially on the AFOSR grant until the summer of 2021. After this he will be fully supported on the AFOSR grant.
- Charlie Lipscomb, MS student who had a 10h/week GRA appointment in the spring of 2020. He helped with the design and development of a magnetic field control system for the chamber, as well as chamber experiments.
- Miles Bengtson, a Ph.D. student who started in the fall of 2017. He has a NDSEG fellowship that covers his salary and came to my lab specifically to perform spacecraft charging experiments. His

dissertation was on using electron sensing to do touchless charge sensing and he supported in 2020 these AFOSR efforts as well. Álvaro is now taking over the electron sensing research having worked side-by-side with Miles and learned his software and hardware skills.

- Ryan Block, an undergraduate researcher who won an Univeristy of Colorado Discovery Learning Apprenticeship program position. This DLA program covers 1/2 of his 10 h/week appointment and the small remainder is covered by this AFOSR grant. He worked closely with Álvaro in the continued development the magnetic field control hardware setup, as well as the Lab View simulation control software. He will continue on this project for the spring of 2021.

	Budget	Actual	Balance
Salaries			
Faculty Salary	$ 28,645.00	$ 28,644.85	$ 0.15
GRA Salary	$ 79,738.00	$ 71,032.10	$ 8,705.90
Benefits	$ 17,703.00	$ 16,830.27	$ 872.73
Salary Totals	$ 126,086.00	$ 116,507.22	$ 9,578.78
Travel			
Travel Totals	$ 10,275.00	$ 2,962.82	$ 7,312.18
Operating Expenses			
Printing	$ 1,000.00	$ 0.00	$ 1,000.00
Cap. Eq.: Residual Gas Analyzer	$ 5,000.00	$ 5,071.00	$ (71.00)
Cap. Eq.: Contactless Voltmeter	$ 7,000.00	$ 0.00	$ 7,000.00
Equipment and Lab Supplies	$ 8,500.00	$ 15,573.58	$ (7,073.58)
Operating Totals	$ 21,500.00	$ 20,644.58	$ 855.42
Tuition/Stipends			
Tuition Totals	$ 30,898.00	$ 18,985.76	$ 11,912.24
Expense Totals	$ 188,759.00	$ 159,100.38	$ 29,658.62
Indirect Totals	$ 78,765.00	$ 75,100.88	$ 3,664.12
Year 3 Project Budget	$ 267,524.00	$ 234,201.26	$ 33,322.74

Figure 1: Comparison between budgeted and actual expenses up to project end in January 31 2021.

4 Budget Update

The 3-year project has total funds of $777,667. The proposal funding rate was $267,524 (1st year), $251,560 (2nd year) and $258,583 for the third year. The cumulative year 1 budget expenses are illustrated in Figure 1 and discussed below.

Overall we followed the expected funding rate closely during the first year and ended up slightly under-spending due to less conference travel costs due to COVID. While the project is budgeted to support the equivalent of 2 full time GRAs for 12 months each year, this first year saw a range of students partially supported on this project while the project staffing is ramping up. See the earlier discussion on students being supported in the Staffing section. In summary, one GRA Kieran Wilson was supported on this full-time for the spring and fall semester, while Álvaro was 20% supported on this program as he has partial support from a graduate fellowship. This allowed him to work side-by-side with senior out-going students and jointly do vacuum chamber experiments. In the spring we supported a MS GRA with a 25% appointment. The summer GRA charges were about the equivalent 70% appointments which allowed the project to support 2 GRAs in full in the fall with the additional 20% support for Álvaro. The result is that for fall 2020 and spring 2021 we have 3 GRAs working on this project. In the fall of 2020 Julian Hammerl started out as the 2nd full-time GRA on this project. He will remain with this project through its completion. Kieran is set to graduate by May 2021. Álvaro's fellowship will end by the end of summer 2021 and he will be the 2nd fully supported GRA. It took some balancing, but I am very pleased with how this project is using the 2 GRA support and stretch it to 3 excited students work on this. As the summer is expected to cover 1.5 GRAs full time as Álvaro is still 50% supported on the fellowship, the plan is to use the 0.5 summer support to partially support a 3rd GRA again in the next AY.

The tuition charged were a little lower than expected as students don't always take a maximum number of classes. Further, Álvaro had his tuition covered through his fellowship this last year which allowed me to stretch the project to include 3 students being fully and partially supported. The 1st project year sending was short $33,322 in total across all spending categories. As conference travel remains very restricted this spring and likely this summer, I plan to use carry forward these funds and hire in an additional GRA for the fall semester on this project. I have received recently very strong interest in a female Ph.D. applicant recently to work on charged astrodynamics recently and these funds would allow me to make her an offer.

Regarding the lab equipment and supplies charges, COVID caused large disruptions and rescheduling of when experiments could be setup and performed due to COVID related campus work-from-home order this spring and summer. In the summer we were able to start to get access again to the lab and commence with the experiment setups. The design of the magnetic field control system continued in the spring, and the hardware started to get purchased and assembled in the fall. However, machine shop access remains intermittent. For the larger equipment ticket items, we did purchase, install and use the residual gas analyzer. We were able to purchase it at the expected cost. The original budget listed an additional piece of expensive equipment, a contactless voltmeter, at $7,000. Over the summer we re-evaluated the status of the vacuum chamber setup, and realized a series of smaller hardware upgrades would enable better research than the contactless voltmeter. This includes better high voltage power supplies that can be directly controlled from a computer. This has allowed us to automate the running of the experiments. These power supplies also have better shielding and more stable voltage outputs for the experiments, and a higher voltage range than prior versions were capable of achieving. While performing experiments that required repeatedly positioning sensors at various points in the chamber over the summer, we found that the open-loop mechanical positioning mechanism we developed had enough slack in it that it impacted the accuracy of the results. Thus, we purchased and are installing new encoders to measure the precise sensor location in the chamber. This will enable micro-meter level position knowledge in the project experiments, essential for several proposal objectives. The new encoders cost about $2,400 and should be installed by February. The residual gas analyzer (RGA) required about $500 in replacement parts. Further, once we got back into the lab this summer and started to run experiments we found that the old chamber lift mechanism was starting to fail. The parts and labour to create a new and better lift mechanism ran about $2,000, but upgrades were completed prior to the fall semester. Thus, despite the periodic campus closures we were able to get the chamber up and running with the new hardware and start the experiments which will run over the next 2 project years. The total equipment and lab expenses for the project matched up very closed with the budgeted year 1 funds with us just slightly under-spending by $855. We feel we have all the expensive equipment setup done at this point to support the experiments to be conducted over the next two project years.

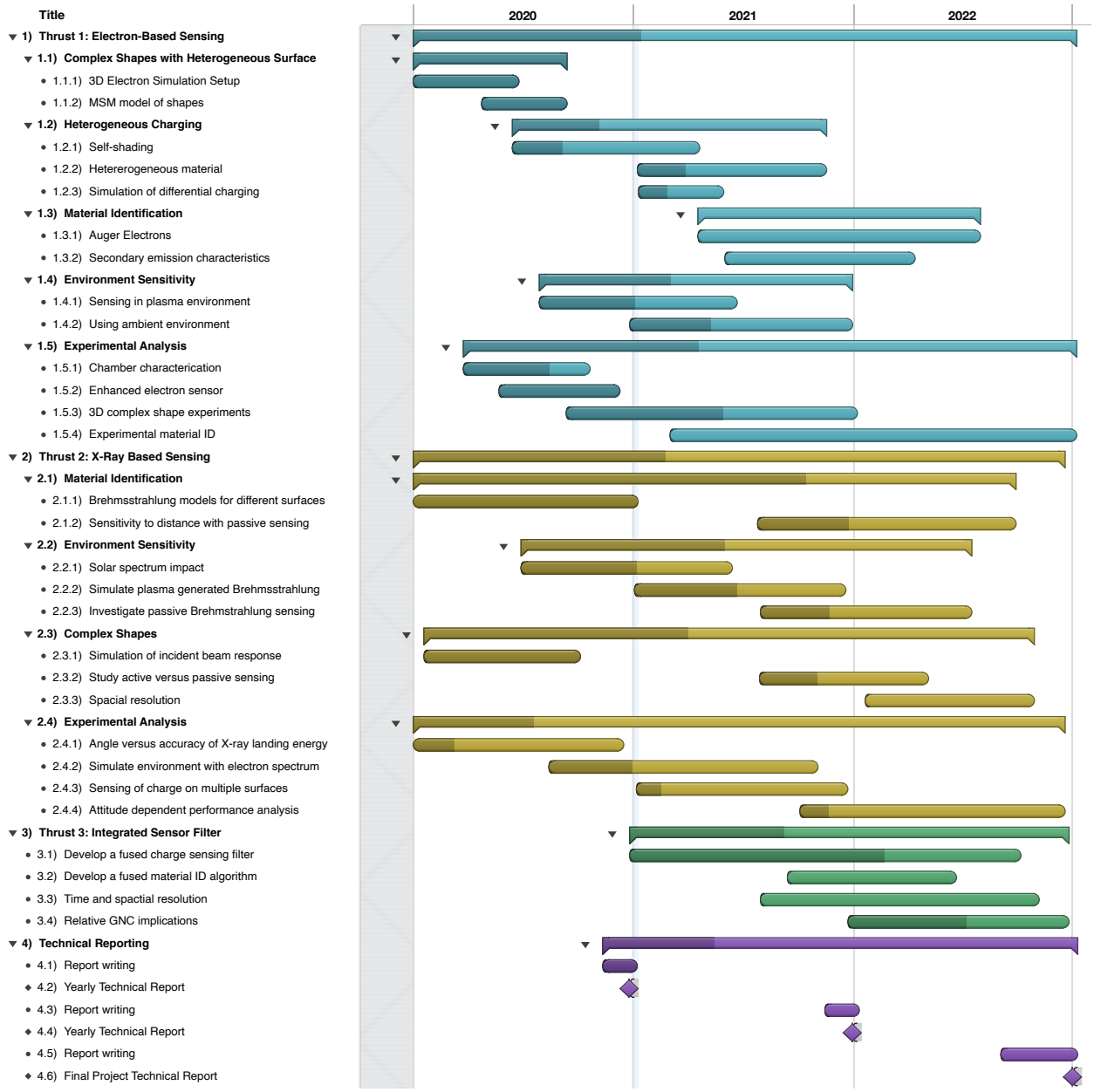

Figure 2: Current Project Schedule (darkened bar indicates degree of completion)

5 Schedule and Project Scope Update

The current project schedule is illustrated in Figure 2. The Proposal tasks are grouped by project thrusts and colored by their status. Most of the year 1 tasks have been completed. Several of the 2nd year tasks have been begun as well. This is due to some COVID chamber access related project task reshuffling, as well as the additional GRA support we enjoyed this year. Because we didn't have lab access this year to do both electron and x-ray sensing experiments, we chose to focus this fall more on the electron sensing work and are now beginning to conduct x-ray sensing experiments this spring. This task shuffle allows us to focus more time on experiments now that we have regular chamber access, which will hopefully continue. I expect by end of year 2 that our tasks across year 1 and year 2 will be completed.

We had to adjust the schedule to deal with the COVID circumstances. Overall I am very pleased with how

the students adjusted and came up with new schedules that kept the project moving forward. If chamber access was not available, or we were dealing with the lift mechanism failures, they regrouped quickly to continue with simulation, analytical and paper writing tasks.

The following sections provide executive summary style discussions on each research thrust area. Where appropriate, we point to the full papers that have been written on this research and are available as downloadable PDF links in Project Publication section 6.

5.1 Thrust 1: Electron Based Sensing

5.1.1 Complex Shapes with Heterogeneous Surface

Evaluating the electric fields in the vicinity of a body is crucial for determining the trajectory of electrons, whether in-bound. Traditional finite element models tend to be quite computationally expensive, limiting their utility. However, in a previous AFOSR grant, we developed a method to rapidly evaluate electric fields and inter-body forces and torques to within 1% error.

A high fidelity method of moments (MOM) finite element setup required approximately 1000 seconds of computation time to find the forces and torques acting between two spacecraft composed of 500 elements each. The equivalent fidelity MSM model required less than 0.2 seconds, for a 10^4 speed up; lower fidelity models can be evaluated much faster still with minimal loss of accuracy.[1] The finite element truth model only needs to be computed once for a structure, and the resulting multi-sphere model is then valid for any future case, including with flexible or time-varying structures, or multiple spacecraft operating in close proximity.[2] This makes MSM ideally suited for faster-than-realtime dynamics propagation, electron trajectory computation, or real-time guidance.

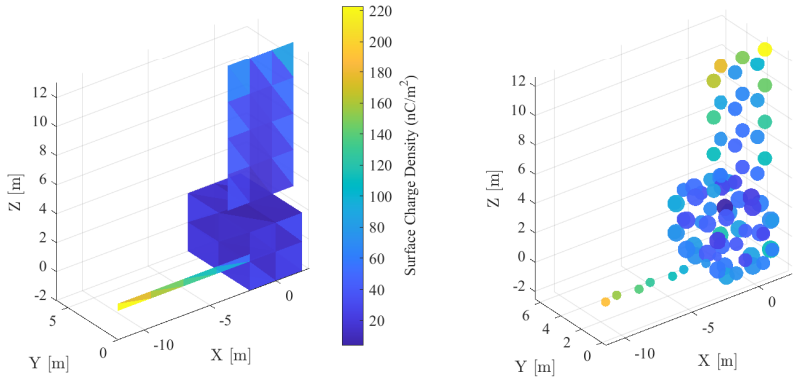

Figure 3: The GOES-R spacecraft approximated as an 80-element MoM finite element model (left) and an 80-sphere MSM model (right). Spheres are colored according to surface charge density.

These models can be developed from any spacecraft geometry (we have developed a library of frequently-used models for generic GEO spacecraft busses), and enable us to rapidly find electron trajectories and spacecraft dynamical interactions. In this 1st project year we developed detailed MSM and method of moments (MoM) models for sample satellites shapes flying in the high altitude region we are considering. Figure 3 shows the GOES-R example where both the MoM and MSM models are illustrated. Having such 3D models of a complex non-spherical shapes support the charged relative motion GNC and charge electron beam landing accuracy studies.

5.1.2 Heterogeneous Charging

Spacecraft design best practices recommend all exterior surface be connected to a common ground to prevent differential charging which can result in hazardous arcing.[3,4] Despite this recommendation, numerous spacecraft are known to become differentially charged and experience arcing (e.g. Ref. 5). This presents an interesting case for touchless sensing because there is not just one target potential to be measured, and the electric fields from differentially-charged spacecraft components may guide the electrons in unexpected directions.

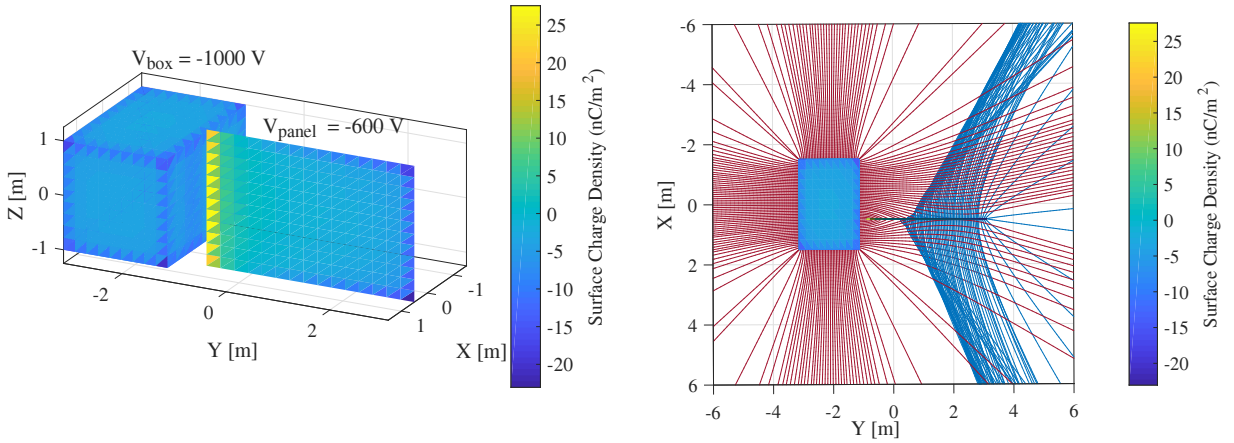

(a) Charge distribution on a differentially-charged spacecraft.

(b) Trajectories of electrons emitted from differentially-charged spacecraft

Figure 4: Differentially-charged spacecraft in which the box is charged to -1000 V and the panel is charged to -600 V.

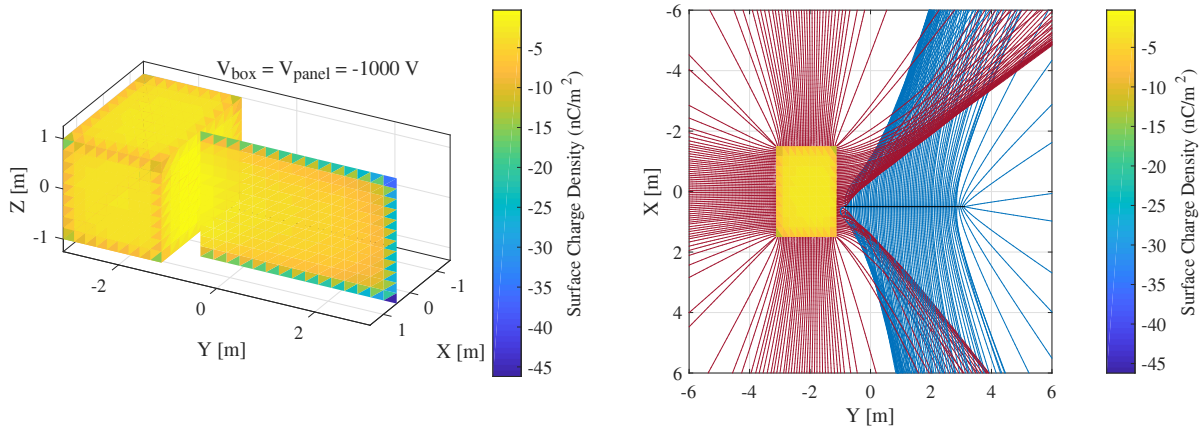

(a) Charge distribution on a homogeneously-charged spacecraft.

(b) Trajectories of electrons emitted from homogeneously-charged spacecraft.

Figure 5: Homogeneously-charged spacecraft in which the box and panel are both charged to -1000 V.

To illustrate this effect, a new simulation was developed for a differentially-charged box-and-panel spacecraft model, in which the box is charged to -1000 V and the panel is charged to -600 V. The MoM model for the differentially-charged craft is shown in Fig. 4(a), and the trajectories of electrons emitted from the craft are shown in Fig. 4(b). For comparison, the electrostatic model and trajectories for a spacecraft of the same shape but homogeneously-charged to -1000 V are shown in Fig. 5. To aid in understanding the trajectories, particles originating on the box are plotted in red, whereas those originating on the panel are plotted in blue. In the homogeneous case, the electrons emitted from the right side of the box are significantly deflected away from the panel. Similarly, those emitted from the panel are also deflected away from the box. In the differential-charging case, however, the electrons emitted from right side of the more negatively-charged box are only slightly perturbed by the presence of the panel. As a result, the population of electrons emitted from the box is visible in a larger spatial region, specifically near the panel edge, than compared the homogeneous-charging case. Those emitted from the panel however, are strongly steered away in the positive Y direction due to the electric field of the box. The electrostatic models show that when the panel is differentially-charged relative to the box, a positive charge resides on the leftward side of the

panel. As a result, electrons originating on the left side of the panel are unable to escape from the surface. The relative location of the sensing craft determines which electron population is measurable. In the differential-charging case, the 600 eV population from the panel is present only in narrower spatial region than the homogeneous case. Both electron populations would be measurable in some specific areas.

When an electron beam is used for active sensing, only those surfaces which are hit with the beam generate electrons, so only the potential on those surfaces are sensed. It would be possible to sense the potential of one surface at a time by deflecting and focusing the electron beam to hit a specific surface, a scenario in which the analysis reported in Sec. 5.2.3.1, is of particular relevance. For the passive sensing case, in which sunlight is used to stimulate photoemission, numerous spacecraft surfaces emit photoelectrons simultaneously, so multiple populations may be present in the electron spectra.

These findings have been validated experimentally for planar systems in Year 1. Future work will validate these complex 3D simulations under different regimes and potential differences.

5.1.3 Material Identification

This task is scheduled to be investigated later in the 2nd project year.

5.1.4 Environmental Sensitivity

One of the main goals of this project is to demonstrate that the touchless sensing concept is feasible given realistic operating conditions. This translates into the question: is the incoming electron flux intense enough to produce a measurable signal? One of the most important factors to consider is the background noise from the plasma environment.

The flux of secondary electrons generated at the surface of the spacecraft by the electron beam can be modeled by the Chung-Everhart energy and the cosine law angular distributions. As a consequence, these particles have an initial energy of just a few eV, and reach the servicer spacecraft with a kinetic energy which is approximately equal to the potential difference between the crafts. The initial emission current can be easily obtained from the secondary electron yield curve of the target material[6]. Typical secondary emission values for aluminum are assumed. The incoming flux of secondary electrons must be superposed to the ambient flux, modeled as a bi-Maxwellian plasma and given by

$$F = \sum_{i=1}^{2} n_i \sqrt{\frac{q}{2\pi T_i m_e}} \frac{qV_S}{k_B T_i} \exp\left(\frac{qV_S}{k_B T_i}\right), \tag{1}$$

where k_B is the Boltzmann constant, m_e is the electron mass, V_S is the spacecraft potential, and other parameters are selected to be representative of storm-time conditions in GEO: n_1 = 0.3 cm^3, T_1 = 4 keV, n_2 = 0.2 cm^3, and T_2 = 7 keV.[7] Two case studies have been analyzed assuming this setup: the electrostatic tractor, and the passive sensing scenario.

For the electrostatic tractor (ET) concept, Ref. 8 provides an example operating condition: a servicing craft of 2 m radius is charged to V_S = 21.4 kV and a target object of radius 0.935 m is charged to V_T = -14.6 kV. The two spacecraft are separated by a distance of 12.5 m. The electron beam energy is E_{beam} = 40 keV and the beam current is I_{beam} = 520 µA. Further, it is assumed that the beam diameter is 20 cm and the beam impacts the target sphere centered on the line of separation. The current of secondary electrons generated for these conditions is 163.0 µA, of which 23.0 µA reach the servicer. Figure 6 shows the electron flux at the sensing craft, including both the ambient plasma and the secondary electron population. The dashed black line shows the expected value of the secondary population energy, equal to the potential difference between the servicing craft and target object: $V_S - V_T = 36.0$ keV. Most importantly, the secondary electrons peak is about 4 orders of magnitude larger than the background noise, and so can be measured.

In the second case study, the target potential is measured using photoelectrons. An operating condition is assumed in which the sensing craft and target object are spheres of 1 m radius, separated by 8 m, with V_S = 200 V and V_T= -50 V. The target is assumed to be a conducting, aluminum sphere with j_{ph} = 40 µA m^2 and $k_B T_{\text{ph}}$ = 2 eV. It is assumed that the half of the target sphere facing the servicing craft is in sunlight. Under these conditions, only 2.8% of the emitted photoelectrons are captured by the sensor on the servicing craft. This percentage is small because photoelectrons are generated on a large area of the target craft, but only a small area maps back to the sensor. Assuming the sunlit area is a circle, the emitted photoelectron current is 126 µA and the current captured by the servicing craft sensor is 3.5 µA. The photoelectron population is modeled as a Maxwellian distribution with a temperature of 2 eV.[9] Figure 7

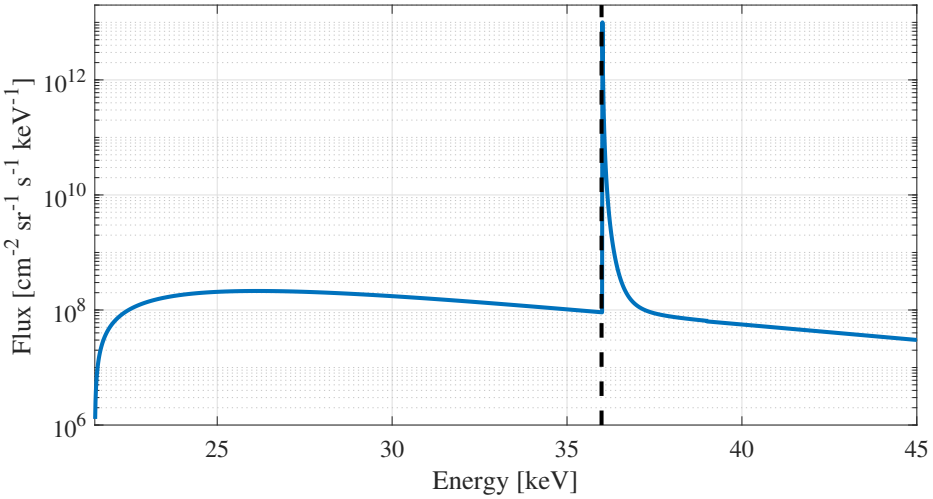

Figure 6: Electron fluxes for the electrostatic tractor remote potential sensing case study. The peak at 36 keV is the electron population from the target, which has been superimposed on a representative plasma background.

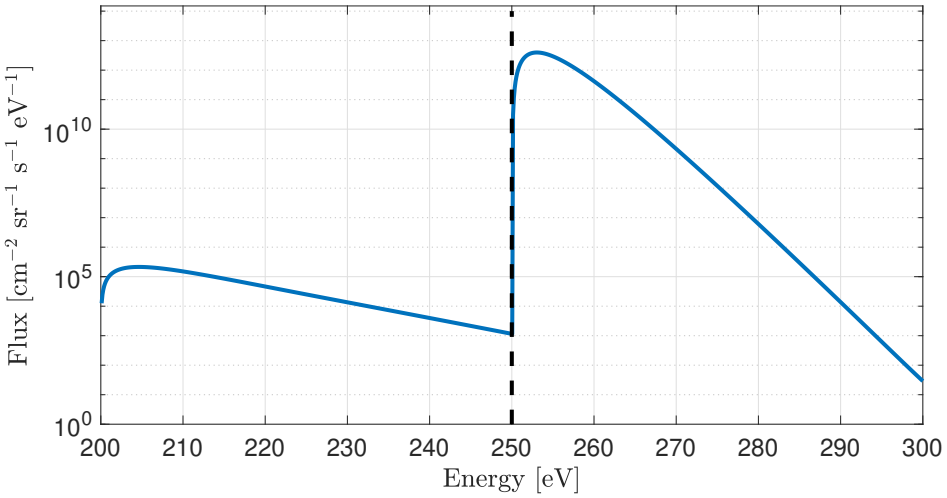

Figure 7: Electron fluxes for the natural charging remote potential sensing case study. The distribution at 250 eV is the electron population from the target object, which has been superimposed on a representative plasma background.

shows the photoelectron population flux superimposed on the bi-Maxwellian background. The dashed black line indicates the potential difference between the two spacecraft. The peak photoelectron flux is several orders of magnitude larger than the background flux, therefore the signal is easily detectable given current energy analyzer capabilities.

In light of this result, touchless potential sensing is feasible for both active and passive scenarios in representative GEO plasma environments. However, these results rely in (i) a spherical spacecraft geometry, (ii) a simplified bi-Maxwellian plasma flux that does not account for the electric field generated by both spacecrafts, and (iii) the assumption that the electric field generated by the beam does not affect the trajectories and energies of the secondary electron flux. In order to conclude this feasibility analysis, it is important to model the previous scenarios with more complex computational frameworks.

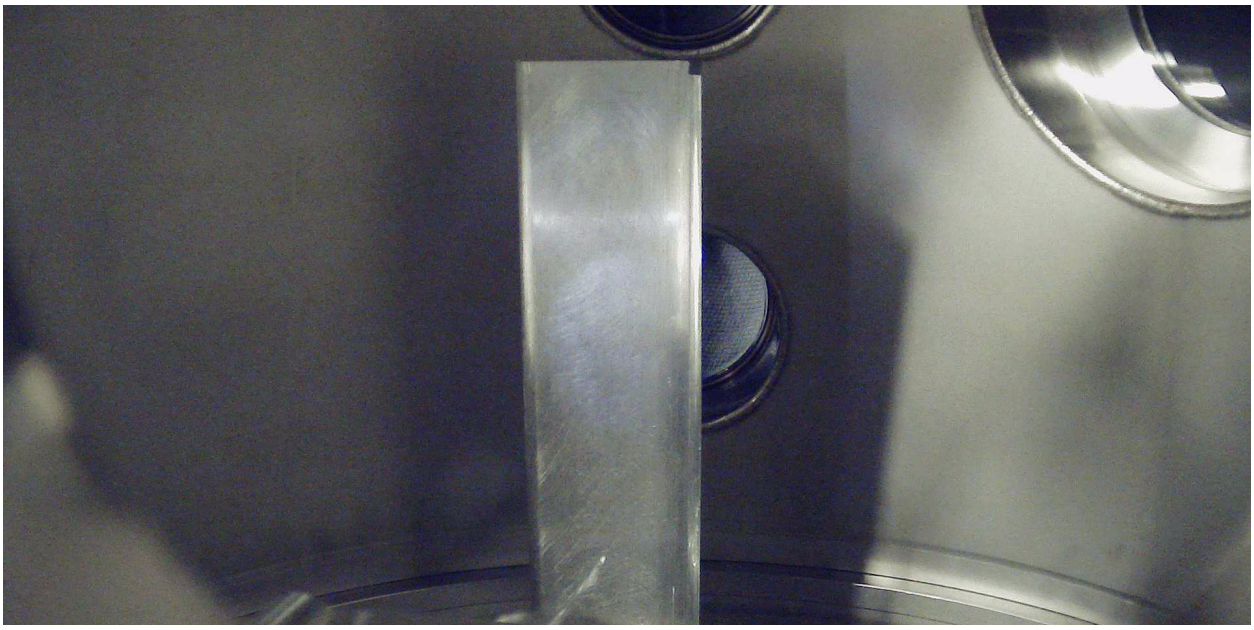

Figure 8: Aluminum bracket in the vacuum chamber illuminated by the VUV light. The circular outline of the VUV light is faintly visible on the bracket.

5.1.5 Experimental Analysis

5.1.5.1 Chamber Characterization

The vacuum chamber has been mostly characterized, and a preliminary report is published as conference paper C-6. Due to the limited access to the lab and matching workshop in summer and fall of 2020 the work on the new encoders and the controlled magnetic fields are still on-going. When this is wrapped up we expect to submit an updated chamber characterization paper to a journal.

5.1.5.2 Enhanced Electron Sensor

The electron sensor development and design was completed in 2020 as has been shown to work well for this project. The chamber characterization paper at C-6 provides more details on its function. This task is considered completed.

5.1.5.3 3D Complex Shape Experiments

The spherical body assumption is commonly applied to spacecraft charging derivations. However, actual spacecraft geometries produce highly inhomogeneous electric fields, effectively acting like lenses that focus and defocus the outcoming flux of secondary electrons. Ultimately, this process determines the density of electrons reaching the detector in the servicer spacecraft, and so must be properly characterized.

To illustrate these ideas, a corner bracket was selected as a test shape. This geometry contains several features which are relevant to spacecraft shapes. It has an exterior corner, which is similar to a box-shaped spacecraft bus. It contains an interior corner similar to a joint between a solar panel and a bus. Finally, edge effects, similar to looking at a solar panel edge-on, are also captured. An aluminum 90° corner bracket 30.48 cm tall with sides 7.62 cm long was used as a target. The object was thoroughly cleaned, mounted on the rotary stage in the vacuum chamber, held at -500 V, and exposed to VUV light to stimulate photoemission. Figure 8 shows the bracket in the vacuum chamber, with circle of VUV light being clearly visible on the center. The RPA, located 30 cm from the target, was used to measure the electron current as the bracket was rotated.

Figure 9 shows the particle trajectories in the horizontal symmetry plane of the bracket computed from a MoM model. The particles are generated with equal spacing along each edge, so the relative density of the particle trajectories (black lines) is representative of what current would be measured by a sensor in a given location. A simulated sensor with the same dimensions as the RPA is swept around the bracket and the number of particles which enter the detector are counted at each angle step. Comparison between the simulated and experimentally measured signal is shown in Fig. 10, with the zero angle being defined by the dashed line and arrow in Fig. 9. Overall, excellent agreement is obtained between the simulation and experiment results. There is a double-peak structure present as the trajectories of particles from the interior faces cross and diverge. The double peak structure is captured well by both the simulation and experiment results. At 180 and 270°, there is a signal increase due to particles emitted from the flat, exterior sides of the bracket. There is a difference of approximately 26% in signal magnitude between the experimentally-measured peaks at these locations. Ideally, both sides of the bracket are identical, so the peaks should also be identical. After discarding alternative explanations, the differences in the surface condition of each side arise as a likely source of error. The bracket was sanded manually, and it is known that variations in surface roughness or the presence of contaminants cause variations in the photoelectron yield.[10] However, overall excellent agreement between simulations and experiments demonstrates that the numerical models capture the physics of electron emission from charged, spacecraft-representative shapes.

With a validated simulation framework, numerical calculations can be applied to a variety of representative spacecraft models. By assuming that all electrons are generated in the Z = 0 plane (a simplification that eases the understanding and interpretation of this phenomenon), results can later be extended to 3D. A representative example is shown in Fig. 11, where a box spacecraft with an antenna dish is modeled. The highest signal regions come from the interior corners where the box and dish are joined, as well as the concave surface of the dish. The lowest signal magnitudes are emitted from the corners of the box and from the edges of the dish. This illustrates the influence of the target spacecraft shape on the density of secondary electron fluxes, and the effects that different geometries induce in the particle trajectories.

To sum up, in Year 1 the MoM numerical simulation framework has been validated for the passive photoemission case, showing that the target spacecraft geometry can have a critical influence in the detected flux of secondary electrons. Year 2 efforts will focus on the effect of 3D shapes in the detection process and explore the active charging scenario.

5.1.5.4 Experimental Material Identification

This effect is scheduled to begin in the 2nd project year.

5.2 Thrust 2: X-Ray Based Sensing

5.2.1 Material Identification

5.2.1.1 Bremsstrahlung models for various materials

Two key methods are used to explore touchless potential sensing in this project: experiments and simulations. Accurate modeling of the x-ray spectrum resulting from a given incident electron energy is therefore crucial to being able to explore x-ray based remote potential measurement in scenarios beyond our experimental facilities. Two components of the x-ray spectrum require separate calculation to simulate the complete electron-induced x-ray spectrum: the discrete energy emission of characteristic radiation, and the bremsstrahlung continuum spectrum.

Characteristic radiation occurs when an incident electron removes an inner shell electron from an atom, at which point an outer shell electron relaxes to fill the vacancy. The energy difference between the two orbitals is released as an x-ray. The energy difference between two orbitals is unique to each element, and as such the emitted photons are characteristic to a specific element and can be used for elemental identification. The characteristic radiation yield, defined as the number of photons of characteristic radiation (from the dominant K_α transitions) generated per incident electron of a specific incident energy can be estimated as

$$I_p = N\left(\frac{E_e}{E_k} - 1\right)^{\alpha} \tag{2}$$

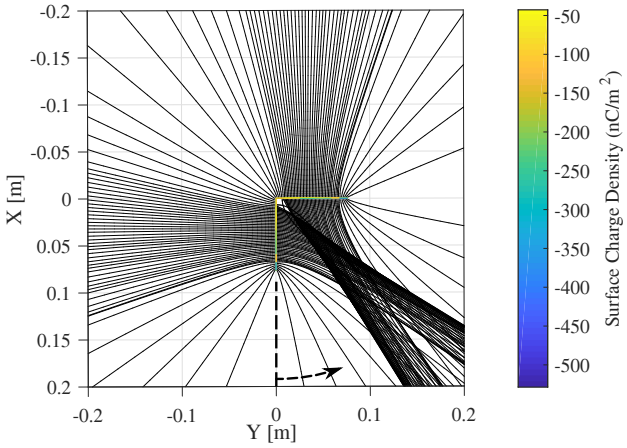

Figure 9: Simulation of electrons emitted from bracket. The dashed line and arrow at the bottom of the figure define the angle referred to in Figure 10.

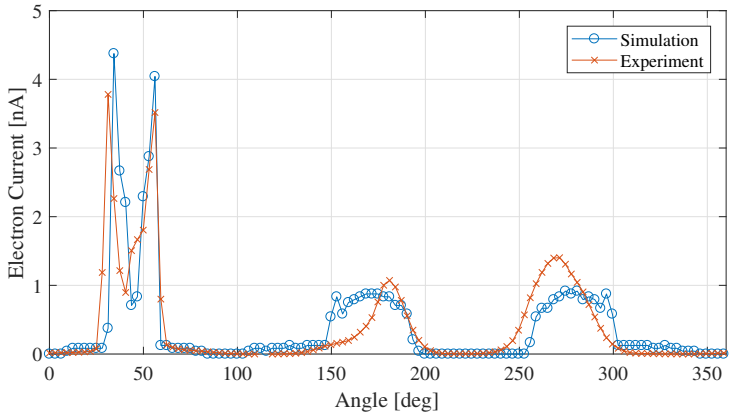

Figure 10: Comparison of experimentally-measured and simulated signal emitted from rotating bracket.

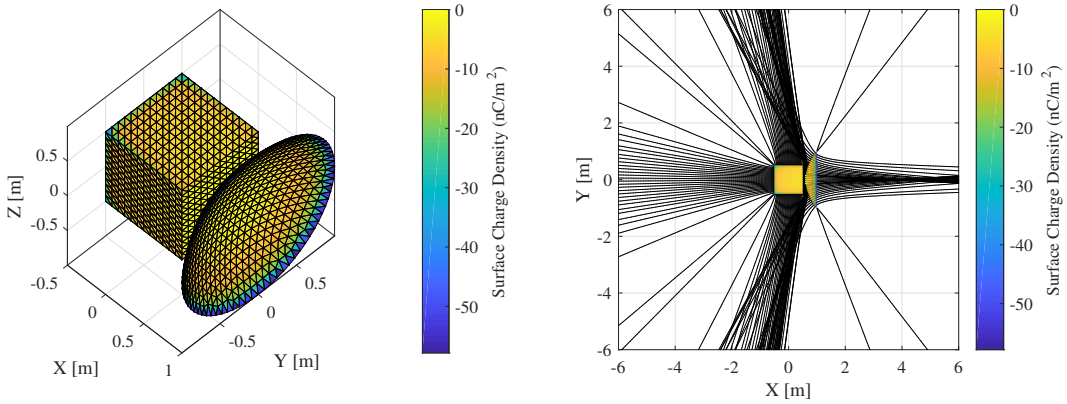

(a) Spacecraft model (b) Trajectories of electrons emitted from spacecraft

Figure 11: Box spacecraft with a parabolic dish antenna.

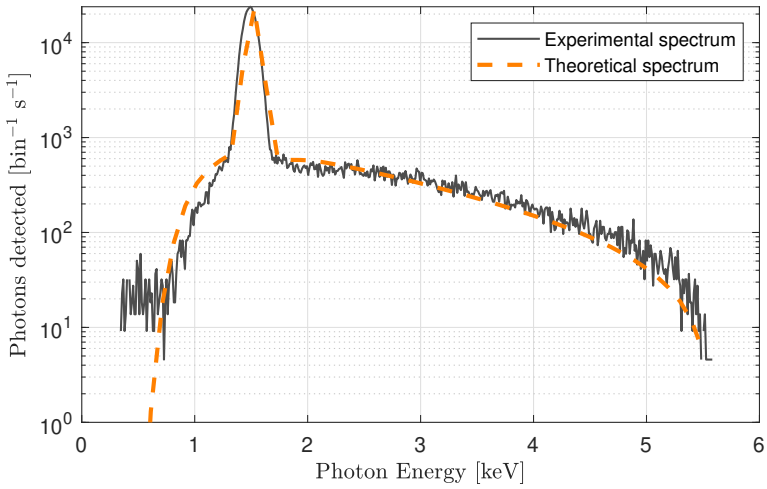

Figure 12: Example of an experimental x-ray spectrum and the theoretical spectrum computed from these models.

where, for aluminum, $N = 1.4 \times 10^{-5}$, $\alpha = 1.63$ and the energy of characteristic emission $E_k = 1.49$, while E_e represents the incident electron energy. Electrons with energy less than E_k are not capable of generating characteristic emission in this transition, so I_p for these cases is zero. For a given number of incident electrons N_e of a specific energy E_e, the expected number of characteristic photons can be computed.[11] This x-ray flux is mono-energetic in nature, but the x-ray detector observes it as a Gaussian peak due to in-sensor spreading effects. These effects can likewise be accounted for if sensor properties are well-known.

5.2.1.2 Sensitivity to Distance with passive sensing

A key initial task for Year 1 was to review relevant literature and select models for simulating x-ray generation. A variety of models are available to simulate the bremsstrahlung spectrum from mono-energetic electrons on thick targets, many of which are provided in review by Reference 12. The electron is assumed to be fully stopped in the target, so a thick target model is used. These models can be divided into two main categories: analytic expressions, often empirically derived from sample data sets, and Monte Carlo-based simulations. While the Monte Carlo simulations can be more accurate than the analytic expressions, they have the disadvantage of requiring significantly more computational resources; the analytic expressions are generally accurate to within 20%, which is not much worse than Monte Carlo simulations, and adequate for the analysis performed here.[12] The equation selected for use here is an empirical fit valid for photons in the 0.5-20 keV range and elements from $Z = 4$ to $Z = 83$, while covering electron energies up to 38 keV. While electron energies considered in this work exceed this value and are subject to reduced accuracy, the results are still considered sufficient for the accuracy desired here.[13]

$$\Delta I = C\sqrt{Z}\frac{E_o - E}{E}\left(-73.90 - 1.2446E + 36.502\ln Z + \frac{148.5E_o^{0.1293}}{Z}\right) \times \left[1 + (-0.006624 + 0.0002906E_o)\frac{Z}{E}\right]\Delta E \quad (3)$$

Using these equations, bremsstrahlung and characteristic radiation yields can be computed for a range of elements, and the output of mixtures of elements can be computed as well. Additional corrections are applied to account for photon absorption in the the detector window and the detector diode.

Implementation of these equations enables rapid simulation of the x-ray spectrum from a given target, with reasonable accuracy as seen in Figure 12. This is a key capability for extending understanding of potential sensing beyond the capabilities of our experimental chamber.

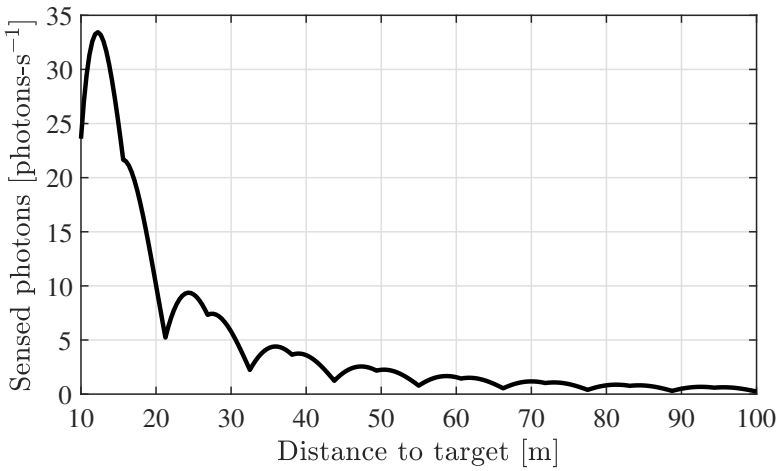

Figure 13: Photon flux sensed at servicer as a result of target-plasma interactions.

5.2.2 Environmental Sensitivity

The passive potential sensing method relies on the change in total number of photons emitted by hot electrons from the ambient plasma impacting the target, and therefore has no sampling requirement to construct a spectrum. Such a method may be effectively executed with tens or hundreds of photons, which may be collected over several seconds. However, using the assumption of even photon flux from the entire surface of the target body, this method would be sensitive to the apparent area of the target facing the servicer. This apparent projected area is a function of the distance between the spacecraft, and also the orientation of the target. Therefore, when comparing the apparent brightness of the target for passive potential estimation, it is important to simultaneously account for target pose and position. Figure 13 illustrates the evolution of a rotating target's apparent brightness due to hot electrons in the ambient plasma. As the target rotates, the projected area seen by the servicer varies by a factor of 3, resulting in periodic variation in the sensed flux.

The x-ray flux is computed from the mean GEO electron spectrum (using the IGE-2006 GEO electron flux model[14]), using equations (3) and (2).

The ambient plasma environment can be used to estimate the electric potential of a neighboring satellite without using an active electron beam to excite x-rays. The x-rays are generated by the ambient electrons in GEO, which possess energies ranging from a few eV to several MeV. Both the characteristic radiation and the bremsstrahlung radiation depend on the energy of the incident electron, and the resulting total x-ray spectrum is a combination of the spectra caused by the ambient electrons with different energies.

A negatively charged spacecraft effectively shifts the energy of the incident electrons. A spacecraft charged to -10kV, for example, will repel any incident electrons with less than 10 keV. Therefore, the electron spectrum will be shifted by 10 keV, and the resulting x-ray spectrum changes accordingly. If the servicing craft can measure the local electron population, then the potential of the target can be inferred by examining the reduction in x-ray emission, as shown in Figure 14.

A conference paper has been presented discussing the findings in C-1. An updated journal article is in preparation (see J-4).

5.2.3 Complex Shapes

5.2.3.1 Simulation of incident beam response

Active spacecraft charging applications rely on the accurate modeling of electron beam dynamics. Past missions have made use of electron beams in space, with some examples being SCATHA[16] or the Electron Drift Instruments at GEOS,[17] Freja,[18] Cluster,[19] and MMS.[20] Particle simulation models have been employed to study the injection and long-term propagation of electron beams in plasma environments.[21–25] The applications here discussed, however, are limited to the *initial expansion* phase, where the beam density is

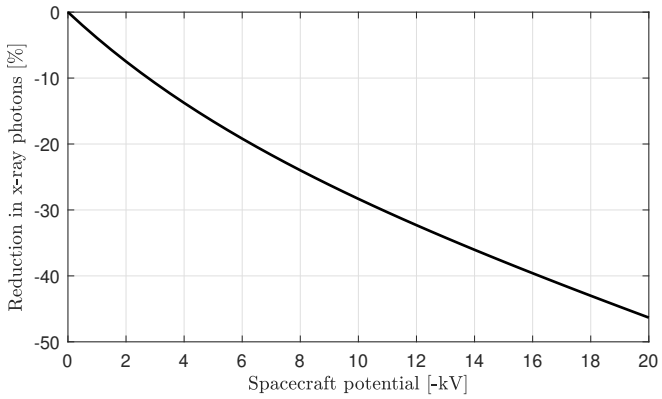

Figure 14: Change in x-ray photon emission due to plasma environment as spacecraft charges.

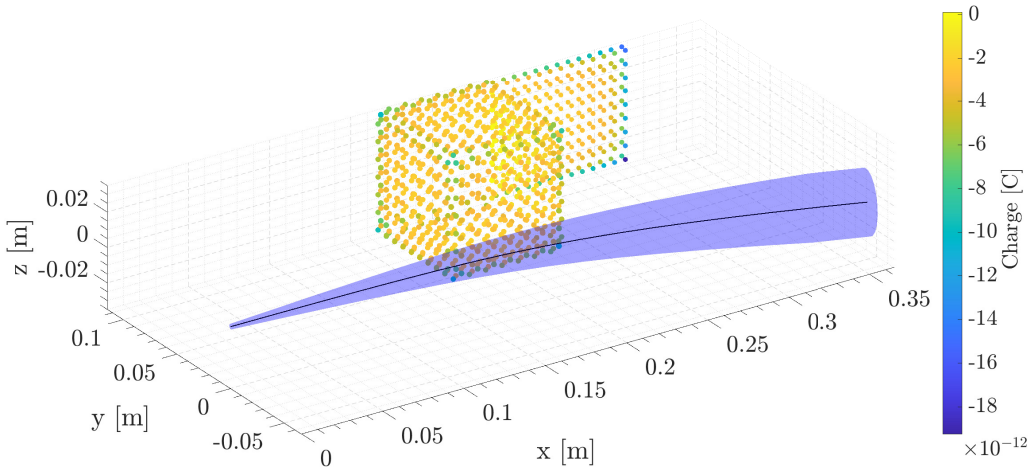

Figure 15: Application of the decoupled electron beam expansion and deflection model with a MSM spacecraft-like electrode at -500 V[15]

much larger than the GEO plasma density and the expansion dynamics are driven by the radial electric field in the beam cross-section.[26] In addition, beam dynamics are significantly affected by the electric fields from nearby charged bodies. This particular environment has motivated the development of a simplified and computationally efficient analytical framework of analysis that decouples electron beam expansion and deflection processes. This model assumes (i) small beam deflection angle θ, (ii) small radial expansion, (iii) axisymmetric distribution of geometry and loads within the beam cross-section, and (iv) negligible plasma interactions. Figure 15 shows a case of application where the electric field created by a charged spacecraft-like electrode induces the deflection of an electron beam. Further details on the mathematical formulation can be consulted in Ref. 15.

This new model is employed in Ref. 15 to quantify the uncertainty in the landing position of the beam in a representative active spacecraft charging scenario. The analysis is designed from the perspective of a servicing spacecraft that directs the beam at a particular area of the target. A total of 702 uncertain variables are considered, with 688 being associated to the Multi-Spheres Model (MSM) that approximates the charge distribution for the two-spacecraft system. Some of the outputs of the analysis are shown in Fig. 16. The initial beam spread angle has the largest influence in the final beam radius, represented in Fig. 16(a), and overcomes beam expansion effects. However, the final beam radius is small in comparison with the spread in the target surface, as shown in Fig. 16(b). The beam centroid has a 93.9% probability of intercepting the target solar panel, represented as a rectangle, while the chances of hitting a 20 cm diameter circle

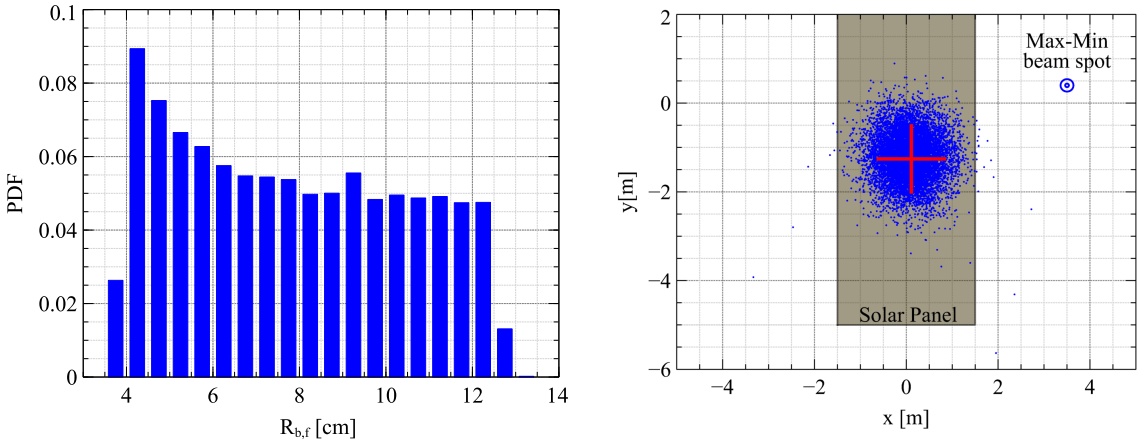

(a) PDF of the final beam radius

(b) Final centroid positions

Figure 16: Result of the Monte Carlo simulation for the study of electron beam landing uncertainties in active spacecraft charging applications[15]

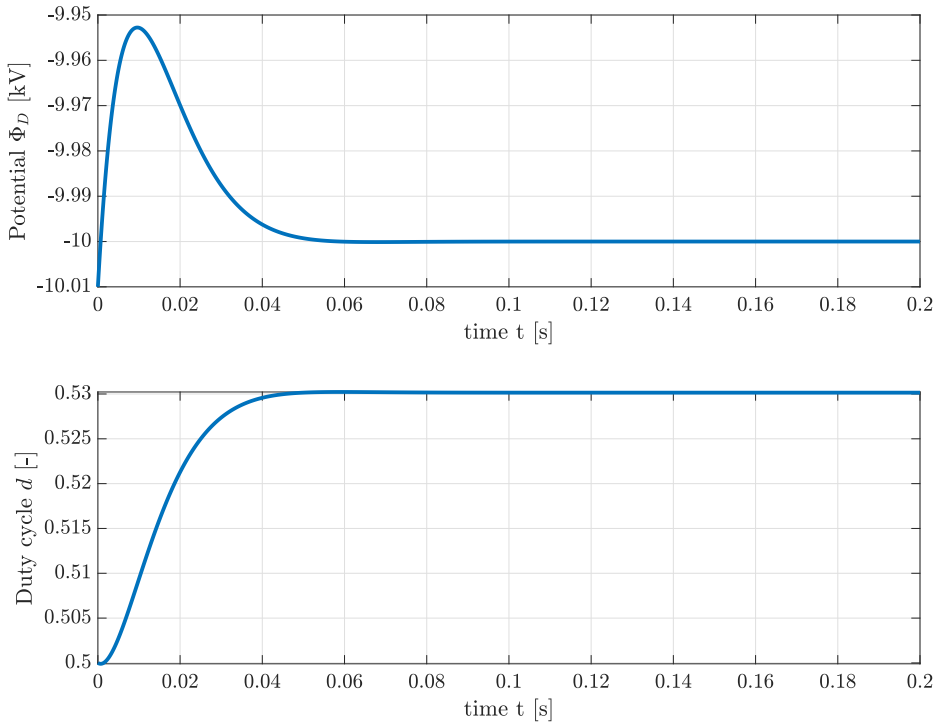

Figure 17: Controlling the duty cycle of the pulsed electron beam to maintain a constant potential of the nearby object.

surrounding the target (red cross) are just a 0.3%. The analysis also provides the beam time-of-flight and energy distributions, which find utility in the prediction of the surface response and in the development of advanced applications involving modulated electron beams.

Thus, a computationally efficient model has been developed to study the electron beam dynamics in active spacecraft charging applications. This work is presented in the project conference paper C-4. Uncertainty quantification tools, such as Monte Carlo and FAST Sensitivity analyses, have been applied to study the spread in the main variables of the problem in a representative scenario. Future space systems dealing with accurate beam pointing and narrow landing energy requirements may consequently benefit from this work. In Year 2, we expected to develop a mixed electron beam model accounting for larger deflection angles. We also plan to study additional cases of interest and build a comprehensive test matrix to guide future developments.

A new research direction has begun in year 1 where we are starting to look at modeling the charged pulsed beam. The motivation and status is as follows. If an electron beam is used to excite x-rays for potential estimation, the target body will accumulate negative charge. However, it might be desired to maintain a constant potential on the nearby satellite during the sensing process. One way to mitigate charging on the neighboring satellite is to use a pulsed electron beam. Instead of using a constant electron beam, the beam energy is periodically increased and decreased. Whenever the beam operates at a high energy, the nearby spacecraft charges negatively. At low beam energies, the spacecraft charges positively due to the high (greater than unity) secondary electron yield.[27] In sunlight the electron beam could be periodically switched off as the photoelectron current dominates and causes the object to charge positively. With the right high energy duty cycle, the target body essentially maintains a constant electric potential. If the servicing satellite senses the potential of the nearby object, the potential estimation can be used to control the duty cycle accordingly (Figure 17).

While significant progress has been made in the theory behind this method, experimental tests will be developed in Year 2 to validate the concept with real-world materials and complications.

5.2.3.2 Active vs passive sensing summary

Methods have been developed to simulate the x-rays generated by both the ambient plasma environment and a mono-energetic electron beam. These can be combined to compare the anticipated yields of active and passive sensing methods.

A nominal electron beam current for a charge control scenario may be on the order of 10 μA. Figure 18 illustrates the relative magnitudes of the bremsstrahlung radiation from the electron beam and the ambient plasma, assumed to be the IGE-2006 mean flux.[14] The solar x-ray spectrum adds only to the characteristic radiation, and has no contribution to the bremsstrahlung continuum, so is not shown here. However, the hot plasma electron flux does contribute to the bremsstrahlung spectrum, but at a level that is approximately 4 orders of magnitude smaller than the beam-induced flux. This makes sense, as the electron beam current in this scenario is 10 μA, while the cumulative plasma current (neglecting charging effects) is approximately 0.7 nA, roughly 3.5 orders of magnitude smaller. Higher energy electrons in the plasma will contribute greater numbers of photons than lower energy electrons.

5.2.4 Experimental Analysis

5.2.4.1 Simulate environment experimentally

A series of experiments were conducted to evaluate the x-ray emission generated by the ambient electron environment. While experiments thus far have been limited in scope, they preliminary suggest high accuracies can be obtained from passive x-ray sensing if the electron environment is known. Figure 19 shows the x-ray spectrum experimentally observed as a result of the broad-spectrum electron gun (see C-5) impacting an aluminum target. Several structures are visible in this plot that are not observed when a mono-energetic spectrum is used, such as the plateau in x-ray counts per bin between 2 and 3 keV. Further studies in year 2 will compare these results to simulations of the anticipated spectrum, and use the broad spectrum electron gun as an environmental noise source for sensing experiments.

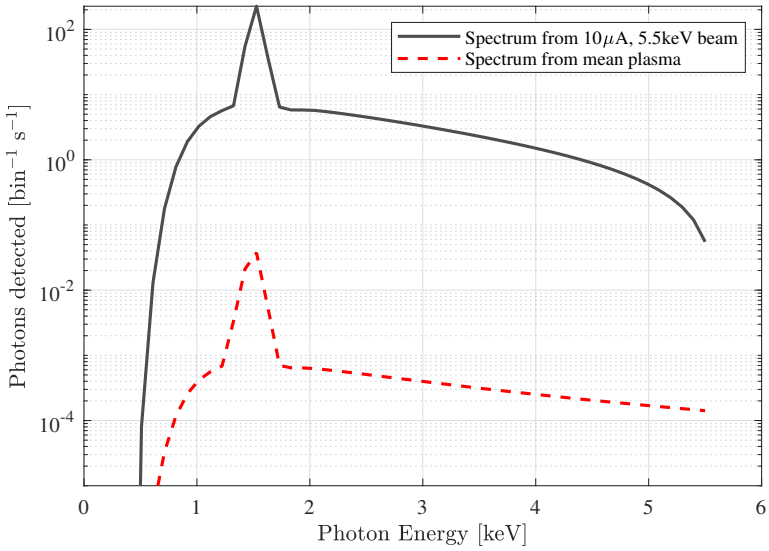

Figure 18: Simulation of sensed x-ray spectrum for a 10 μA electron beam and ambient plasma electron fluxes, using the IGE-2006 mean flux. The target is assumed to be an isotropically emitting point source equivalent to a 5 m^2 aluminum spacecraft.

5.2.4.2 Broad spectrum electron gun update

The broad spectrum electron gun has been crucial to experimentally validating methods for estimating electrostatic potential using the ambient plasma environment. A new version of this device has been built as shown in Figure 21, as well as tested and characterized as discussed in C-5. Figure 22 illustrates the energy distribution of electrons emerging from the broad spectrum electron gun, and a nominal GEO electron spectrum for comparison.

The tunable nature of the broad spectrum electron gun design ensures that any desired electron spectrum can be emulated, allowing experimental simulation of on-orbit electron fluxes for charging and charge sensing studies.

Now that this unique capability has been proven out through year 1 development efforts, year 2 can focus on utilizing the broad spectrum electron gun to experimentally simulate the space environment. A conference paper has been published on the development and testing of this broad-spectrum electron gun (see C-5).

5.3 Thrust 3: Integrated Sensor Filter

5.3.1 Develop Fused Charge Sensing Filter

Both the electron and x-ray methods have unique strengths, which can be combined to improve the accuracy of the overall potential estimate. We have performed experiments and implemented an adaptive Kalman Filter to fuse measurements from both instruments. As the target plate used in experiments rotates, the electrons follow trajectories dictated by the electric field around the plate whether the result of secondary emission or photoelectric emission. Therefore, signal availability and SNR is a function of the attitude of the plate. The x-ray method is less sensitive to target attitude, but tends to produce less accurate results in general (see Figure 23 for an example of the uncertainty in each measurement as a function of target plate angle).

Ultimately, the x-ray method is able to provide consistent uncertainties of 150V (under these conditions) for most angles, while the electron method provides uncertainties of less than 10V at a subset of angles. Therefore, combining these measurements enables a signal with wide availability but limited accuracy (the x-ray method) to be periodically updated by a much higher accuracy method (the electron-based method) whenever the relative geometry is oriented to provide a signal. A filter was developed to fuse potential

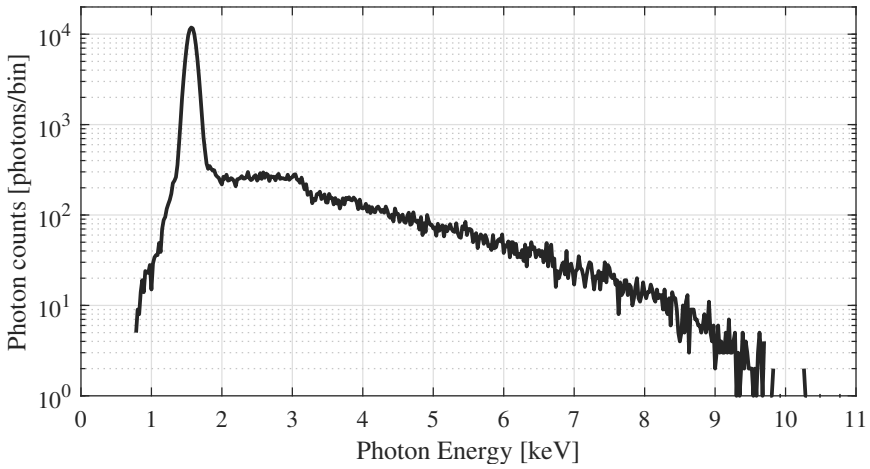

Figure 19: X-ray spectrum resulting from broad-spectrum electron gun with 10keV maximum energy.

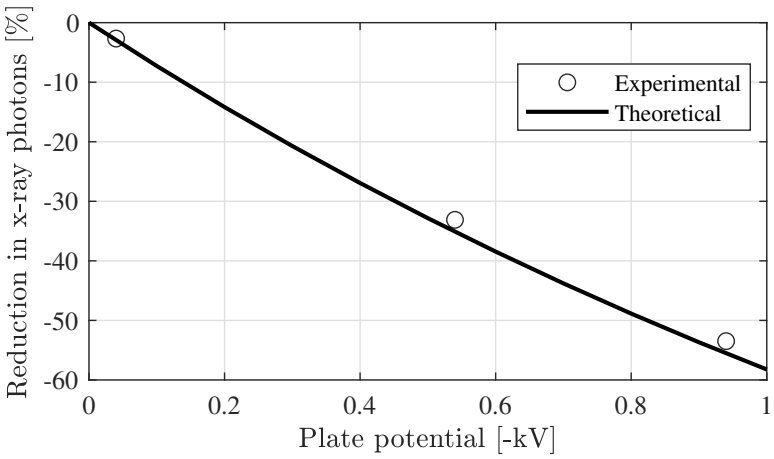

Figure 20: Using the broad spectrum electron gun to validate electrostatic sensing using only the ambient plasma.

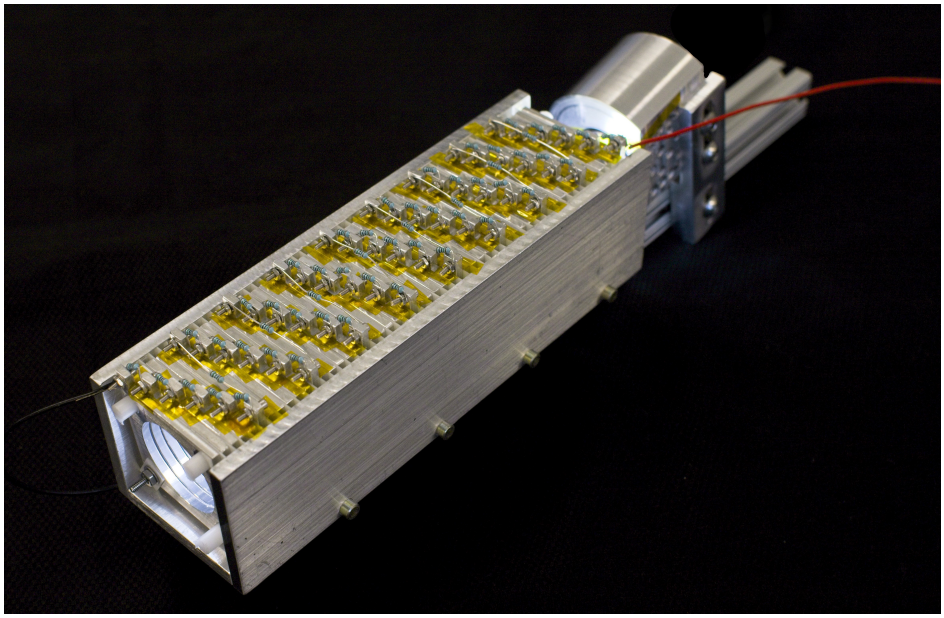

Figure 21: Broad spectrum electron gun.

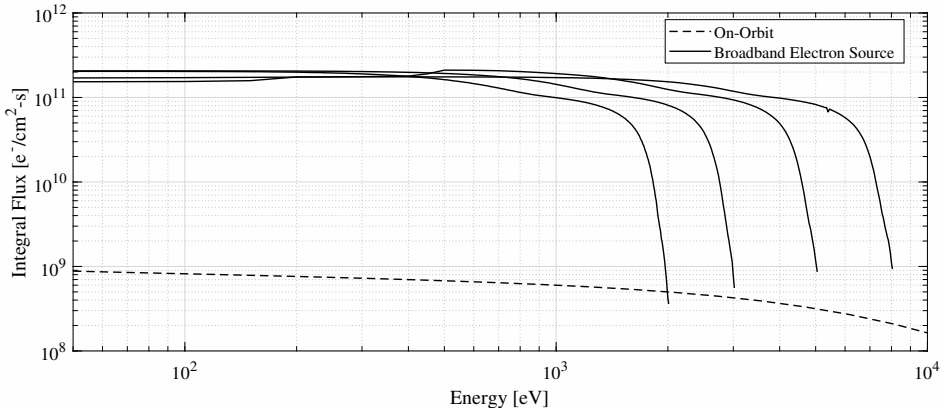

Figure 22: Example output spectrum from the broad-spectrum electron gun up to 8 keV compared to data from GEO.[28]

estimates from both methods and uncertainty associated with each, through an adaptive Kalman Filter which helps compensate for unknown charging system dynamics. An example of filter performance with a simulated scenario with eclipse-like charging transients shows the adaptive filter tracking the reference signal much more closely than the steady state Kalman filter design.

This work has provided insight into how these two complimentary methods could be combined, and some insight into how they may be used in an on-orbit scenario. Future work in this area will improve filter fusion performance, and provide means of improving potential estimates by filtering the raw spectral signals obtained by the instruments. A conference paper on the year 1 work is presented in C-2 and an expanded discussion is submitted to the IEEE journal (see J-2).

5.3.2 Develop a Fused Material ID Algorithm

This task is scheduled to be investigated later in the 2nd project year.

5.3.3 Time and Spacial Resolution

This task is scheduled to be investigated later in the 2nd project year.

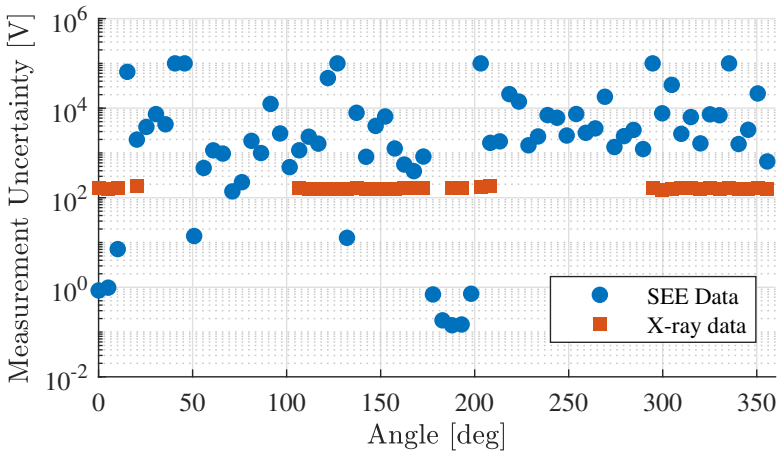

Figure 23: Uncertainties in potential estimation for both methods

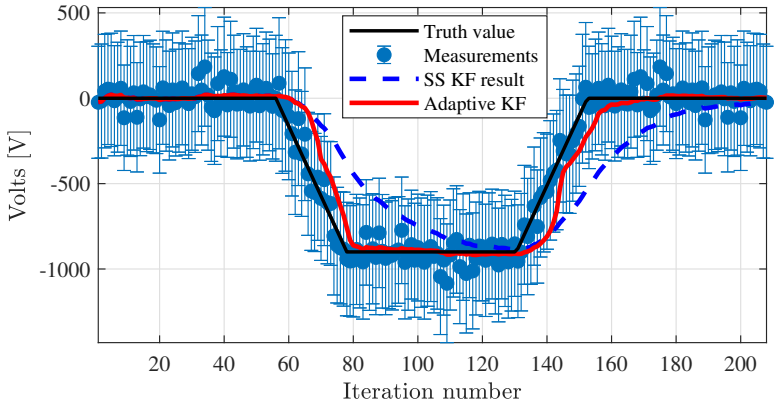

Figure 24: Application of adaptive filter to simulated data with eclipse-like transients.

5.3.4 Relative GNC Implications

The impact of electrostatic perturbations is a previously unconsidered aspect of proximity operations, despite the fact that spacecraft – and debris objects – can naturally charge to tens of kV at GEO. In a scenario where a servicer is approaching debris or an inoperative satellite, electrostatic interactions can result in quite dramatic torques acting on a target body. Autonomous rendezvous is typically a slow process, which allows the torques to accumulate into high rotational rates. Furthermore, as the servicer will typically follow a target-body fixed approach trajectory, the servicer will need to expend considerable fuel accelerating to match the rotating target.

Analysis was performed with a target spacecraft modeled after NOAA's next-generation GEO weather satellites, in particular the GOES-R bus. After estimating mass and inertia properties from publicly available data, a Method of Moments (MOM) model was developed, and used as a basis for a Multi-Sphere Method (MSM) model that could be evaluated quickly enough for dynamics computations. A similar process was performed for a notional servicer, based on the Northrop Grumman MEV-1 vehicle. Figure 26 illustrates the impact that electrostatic perturbations can have on a static hold scenario, where the servicer maintains a fixed position 10 meters from the target as might be required for pre-servicing inspections.

Ultimately this work has shown that these previously neglected perturbations can be significant for high earth orbits regarding the relative motion station keeping fuel usage. This result has prompted interest from industry. Integration with remote potential sensing further enables these perturbing dynamics to be accounted for, which yields more efficient, safer trajectories. Initial versions of these guidance and control

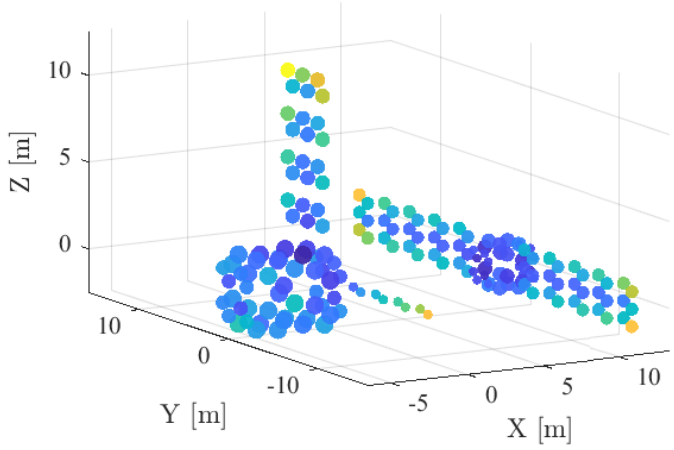

Figure 25: Servicer (right) at a 10 meter hold point relative to the target (left), both craft at 0 kV.

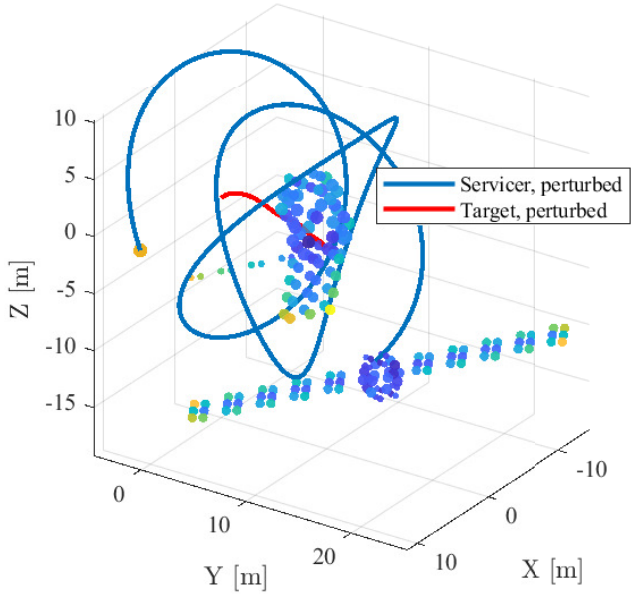

Figure 26: Results of servicer holding a fixed position relative to a target for a 5 hour hold, shown in the Hill frame. Electrostatic torques result in a significant tumble being imparted to the target (both SC at -10kV), despite it having no initial rotation. Only electrostatic perturbations acted on the target.

algorithms have been developed to capitalize on knowledge of the target potential provided by the x-ray and electron-based methods, and over the coming year those algorithms will be further extended and improved. This will include evaluating sensitivity to target potential measurements, and integrating simulations of target electron and x-ray spectra. These perturbations can even be used to counteract other perturbations, like SRP, during proximity operations, which enables rendezvous to be conducted more safely.

This work has been published in this conference paper C-3 and has been submitted to JSR as a journal paper (see J-1). New work has been written up to be presented in the upcoming IEEE conference in C-7.

The year 1 work also included a new study on the charged relative position station keeping taking into account uncertainty in the target voltage measurement, as well as the impact of the three-dimensional target shape. Prior work in Ref. 29 only considered sphere on sphere interactions. The 3D MSM shapes developed in this project are being used to simulate how the relative orientation, as well as the potential measurement uncertainties found with touchless charging, will impact the stability of the charged relative motion. This conference paper abstract on this work (C-8) has been accepted at the upcoming virtual 8th European Conference on Space Debris.

6 Associated Publications

The following comprehensive list contains the research grant related papers that have been created thus far, or are in progress. When available, the paper title links directly to a public PDF of this paper, and the DOI number is a hyperlink to the publisher web page.

6.1 Conference Papers

C-1. K. Wilson and H. Schaub, "Environmental X-Ray Considerations For Bremsstrahlung-Based Surface Potential Determination," AIAA SciTech Forum, Orlando, Florida, Jan. 6–10, 2020, *AIAA Atmospheric and Space Environments Best Paper Award winner*
doi:10.2514/6.2020-0049

C-2. K. Wilson, M. Bengtson and H. Schaub, "Hybrid Method of Remote Sensing of Electrostatic Potential for Proximity Operations," IEEE Aerospace Engineering Conference, Big Sky, Montana, March 7–14, 2020

C-3. K. T. Wilson and H. Schaub, "Impact Of Electrostatic Perturbations On Proximity Operations In High Earth Orbits," AAS/AIAA Astrodynamics Specialist Conference, Lake Tahoe, CA, Aug. 9–13, 2020.

C-4. Á. Romero Calvo, G. Cano Gómez and H. Schaub, "Electron Beam Expansion And Deflection Uncertainty For Active Charging Applications," AIAA SciTech, Nashville, TN, Jan. 11–15, 2021.
doi:10.2514/6.2021-1540

C-5. M. T. Bengtson, K. T. Wilson and H. Schaub, "Broad-Spectrum Electron Gun for Laboratory Simulation of Orbital Environments," AIAA SciTech, Nashville, TN, Jan. 11–15, 2021.
doi:10.2514/6.2021-1539

C-6. K. T. Wilson, M. T. Bengtson, J. Maxwell, Á. Romero Calvo and H. Schaub, "Characterization of the ECLIPS Space Environments Simulation Facility," AIAA SciTech, Nashville, TN, Jan. 11–15, 2021.
doi:10.2514/6.2021-1538

C-7. K. T. Wilson and H. Schaub, "Constrained Guidance For Spacecraft Proximity Operations Under Electrostatic Perturbations" Accepted to IEEE Aerospace Engineering Conference, Big Sky, Montana, March 6–13, 2021

C-8. J. Hammerl and H. Schaub, "Effects of Electric Potential Uncertainty on Electrostatic Tractor Relative Motion Control, " Accepted to 8th European Conference on Space Debris, Darmstadt, Germany, April 20–23, 2021

6.2 Journal Papers

J-1. K. T. Wilson and H. Schaub, "Impact of Electrostatic Perturbations on Proximity Operations in High Earth Orbits," Submitted to *Journal of Spacecraft and Rockets*

J-2. K. T. Wilson, M. Bengtson and H. Schaub, "Remote Electrostatic Potential Sensing for Proximity Operations: Comparison and Fusion of Methods," Submitted to *AIAA Journal of Spacecraft and Rockets*.

J-3. M. Bengtson and H. Schaub, "Electron-Based Touchless Potential Sensing of Shape Primitives and Differentially-Charged Spacecraft," In preparation for *Journal of Spacecraft and Rockets*

J-4. K. T. Wilson, J. Hammerl, H. Schaub, "Space environmental x-ray considerations for bremsstrahlung-based surface potential determination," In preparation for *Journal of Space Weather*

7 Project Conclusions and Outlook

I'm very pleased with the progress during the first project year. The GRA support was well managed across a mid-semester start-up and lead to additional research support for this project. The senior students are ramping up the new students and the general research climate is full of excitement about this work. I will continue to seek means to stretch the GRA funds to include more than graduate and undergraduate researchers in this project. COVID definitely impacted the project as it limited the research lab access where the vacuum chamber facility resides. However, the impacts are well-managed and are resulting in some shuffling of when experiments will be conducted, and is not impacting the overarching project goals thus far. We are well-positioned to complete all the year 1 and 2 tasks by the end of the second project year. Budget wise we ended up slightly under-spending because of reduced conference travel and student support costs. The plan here is to use the carry-over funds to recruit an additional student to this project for next fall.

We are well-poised now to do a lot of the harder project experimental tasks over this year. In the first year we took advantage of the lab down time get ahead on analysis and software development. The chamber hardware and software changes are functioning well and new x-ray sensing experiments are already underway. While some conferences we planned to attend are canceled, as with the spacecraft charging conference, we are seeking alternate avenues to present our work as as the AIAA Atmospheric and Space Environments section at SciTech, as well as the astrodynamics conferences regarding the charged guidance, navigation and control work. Our plan is to continue to present this research at conferences even it they are held in a virtual format.[30]

References

[1] Hughes, J. and Schaub, H., "Heterogeneous Surface Multisphere Models using Method of Moments Foundations," *Journal of Spacecraft and Rockets*, Vol. 56, No. 4, August 2019, pp. 1259–1266, doi:10.2514/1.A34434.

[2] Maxwell, J., Wilson, K. T. H., Ghanei, M., and Schaub, H., "Multisphere Method for Flexible Conducting Space Objects: Modeling and Experiments," *AIAA Journal of Guidance, Control, and Dynamics*, Vol. 57, No. 2, Aug. 19–23 2020, pp. 225–234, doi:10.2514/1.A34560.

[3] Garrett, H. B. and Whittlesey, A. C., *Guide to mitigating spacecraft charging effects*, Vol. 3, John Wiley & Sons, 2012.

[4] Purvis, C. K., Garrett, H. B., Whittlesey, A., and Stevens, N. J., "Design guidelines for assessing and controlling spacecraft charging effects," 1984.

[5] Ferguson, D., White, S., Rast, R., and Holeman, E., "The Case for Global Positioning System Arcing and High Satellite Arc Rates," *IEEE Transactions on Plasma Science*, Vol. 47, No. 8, 2019, pp. 3834–3841.

[6] Draine, B. and Salpeter, E., "On the physics of dust grains in hot gas," *The Astrophysical Journal*, Vol. 231, 1979, pp. 77–94.

[7] Davis, V., Gardner, B., and Mandell, M., "Nascap-2k Version 4.3 Users Manual," Tech. report, LEIDOS, San Diego, CA, 2016.

[8] Hogan, E. and Schaub, H., "Space Weather Influence on Relative Motion Control using the Touchless Electrostatic Tractor," *Journal of Astronautical Sciences*, Vol. 63, No. 3, 2016, pp. 237–262, doi:10.1007/s40295-016-0090-4.

[9] Grard, R. J., "Properties of the satellite photoelectron sheath derived from photoemission laboratory measurements," *Journal of geophysical research*, Vol. 78, No. 16, 1973, pp. 2885–2906.

[10] Feuerbacher, B. and Fitton, B., "Experimental investigation of photoemission from satellite surface materials," *Journal of Applied Physics*, Vol. 43, No. 4, 1972, pp. 1563–1572.

[11] Castellano, G., Osán, J., and Trincavelli, J., "Calculation of x-ray bremsstrahlung and characteristic line emission produced by a Maxwellian electron distribution," *Journal of Physics. D, Applied Physics*, Vol. 15, No. 5, 1982.

[12] Trincavelli, J. and Castellano, G., "The prediction of thick target electron bremsstrahlung spectra in the 0.25–50 keV energy range," *Spectrochimica Acta Part B: Atomic Spectroscopy*, Vol. 63, No. 1, 2008, pp. 1 – 8.

[13] Castellano, G., Osán, J., and Trincavelli, J., "Analytical model for the bremsstrahlung spectrum in the 0.25–20 keV photon energy range," *Spectrochimica Acta Part B: Atomic Spectroscopy*, Vol. 59, No. 3, 2004, pp. 313 – 319.

[14] Sicard-Piet, A., Bourdarie, S., Boscher, D., Friedel, R. H. W., Thomsen, M., Goka, T., Matsumoto, H., and Koshiishi, H., "A new international geostationary electron model: IGE-2006, from 1 keV to 5.2 MeV," *Space Weather*, Vol. 6, No. 7, 2008, doi:10.1029/2007SW000368.

[15] Romero Calvo, Á., Schaub, H., and Cano Gómez, G., "Electron beam expansion and deflection uncertainty for active spacecraft charging applications," *AIAA SciTech Conference*, Nashville, TN, Jan. 11–15 2021, doi:10.2514/6.2021-1540.

[16] Olsen, R. and Cohen, H., "Electron beam experiments at high altitudes," *Advances in Space Research*, Vol. 8, No. 1, 1988, pp. 161 – 164.

[17] Melzner, F., Metzner, G., and Antrack, D., "The GEOS electron beam experiment," *Space Science Instrumentation*, Vol. 4, 1978, pp. 45–55.

[18] Paschmann, G., Boehm, M., Höfner, H., Frenzel, R., Parigger, P., Melzner, F., Haerendel, G., Kletzing, C. A., Torbert, R. B., and Sartori, G., "The Electron Beam Instrument (F6) on Freja," *Space Science Reviews*, Vol. 70, No. 3, Nov 1994, pp. 447–463.

[19] Paschmann, G., Melzner, F., Frenzel, R., Vaith, H., Parigger, P., Pagel, U., Bauer, O. H., Haerendel, G., Baumjohann, W., Scopke, N., Torbert, R. B., Briggs, B., Chan, J., Lynch, K., Morey, K., Quinn, J. M., Simpson, D., Young, C., Mcilwain, C. E., Fillius, W., Kerr, S. S., Mahieu, R., and Whipple, E. C., "The Electron Drift Instrument for Cluster," *Space Science Reviews*, Vol. 79, No. 1, Jan 1997, pp. 233–269.

[20] Torbert, R. B., Vaith, H., Granoff, M., Widholm, M., Gaidos, J. A., Briggs, B. H., Dors, I. G., Chutter, M. W., Macri, J., Argall, M., Bodet, D., Needell, J., Steller, M. B., Baumjohann, W., Nakamura, R., Plaschke, F., Ottacher, H., Hasiba, J., Hofmann, K., Kletzing, C. A., Bounds, S. R., Dvorsky, R. T., Sigsbee, K., and Kooi, V., "The Electron Drift Instrument for MMS," *Space Science Reviews*, Vol. 199, No. 1, Mar 2016, pp. 283–305.

[21] Okuda, H. and Berchem, J., "Injection and propagation of a nonrelativistic electron beam and spacecraft charging," *Journal of Geophysical Research: Space Physics*, Vol. 93, No. A1, 1988, pp. 175–195.

[22] Okuda, H. and Ashour-Abdalla, M., "Propagation of a nonrelativistic electron beam in three dimensions," *Journal of Geophysical Research: Space Physics*, Vol. 95, No. A3, 1990, pp. 2389–2404.

[23] Okuda, H. and Ashour-Abdalla, M., "Injection of an overdense electron beam in space," *Journal of Geophysical Research: Space Physics*, Vol. 95, No. A12, 1990, pp. 21307–21311.

[24] Winglee, R. M., "Simulations of pulsed electron beam injection during active experiments," *Journal of Geophysical Research: Space Physics*, Vol. 96, No. A2, 1991, pp. 1803–1817.

[25] Koga, J. and Lin, C. S., "A simulation study of radial expansion of an electron beam injected into an ionospheric plasma," *Journal of Geophysical Research: Space Physics*, Vol. 99, No. A3, 1994, pp. 3971–3983.

[26] Gendrin, R., "Initial expansion phase of an artificially injected electron beam," *Planetary and Space Science*, Vol. 22, No. 4, 1974, pp. 633 – 636.

[27] Lai, S. T., *Fundamentals of Spacecraft Charging: Spacecraft Interactions with Space Plasmas*, Princeton University Press, 2011.

[28] Thomsen, M., Denton, M., Lavraud, B., and Bodeau, M., "Statistics of plasma fluxes at geosynchronous orbit over more than a full solar cycle," *Space Weather*, Vol. 5, No. 3, 2007.

[29] Hogan, E. and Schaub, H., "Relative Motion Control for Two-Spacecraft Electrostatic Orbit Corrections," *AIAA Journal of Guidance, Control, and Dynamics*, Vol. 36, No. 1, Jan. – Feb. 2013, pp. 240–249, doi:10.2514/1.56118.

[30] Schaub, H. and Junkins, J. L., *Analytical Mechanics of Space Systems*, AIAA Education Series, Reston, VA, 4th ed., 2018, doi:10.2514/4.105210.